Leading particles and diffraction dissociation in 150-GeV/c $\pi^- p$ interactions

D. Brick, D. Fong,* M. Heller,† A. M. Shapiro, and M. Widgoff
Brown University, Providence, Rhode Island 02912

F. Bruyant
CERN, Geneva 23, Switzerland

P. Lucas
Duke University, Durham, North Carolina 27706

D. Bogert and M. Johnson
Fermilab, Batavia, Illinois 60510

R. Burnstein, C. Fu,§ D. Petersen,‖ M. Robertson,¶ and H. Rubin
Illinois Institute of Technology, Chicago, Illinois 60616

R. Sard, A. Snyder,** and J. Tortora††
University of Illinois, Urbana, Illinois 61801

E. D. Alyea, Jr.
Indiana University, Bloomington, Indiana 47401

C.-Y. Chien, A. Pevsner, and R. Zdanis
Johns Hopkins University, Baltimore, Maryland 21218

F. Barriero,* O. Benary,‡‡ J. F. Brau,§§ J. Grunhaus,‖‖ E. S. Hafen, R. I. Hulsizer, U. Karshon,¶¶ V. Kistiakowsky, A. Levy,‖‖ A. Napier,*** I. A. Pless, J. P. Silvermann,††† P. C. Trepagnier, J. Wolfson,‡‡‡ and R. K. Yamamoto
Laboratory for Nuclear Science and Department of Physics, Massachusetts Institute of Technology, Cambridge, Massachusetts 02139

H. Cohn
Oak Ridge National Laboratory, Oak Ridge, Tennessee 37830

P. F. Jacques, T. C. Ou, R. J. Plano, and T. L. Watts
Rutgers University, New Brunswick, New Jersey 08903

E. Brucker, E. Koller, P. Stamer, and S. Taylor
Stevens Institute of Technology, Hoboken, New Jersey 07030

W. Bugg, G. Condo, T. Handler, and E. Hart
University of Tennessee, Knoxville, Tennessee 37916

H. Kraybill, D. Ljung,‡‡‡ T. Ludlam,§§§ and H. D. Taft
Yale University, New Haven, Connecticut 06520

(Received 15 March 1979; revised manuscript received 12 October 1979)

Diffraction dissociation of both the beam and target particles has been observed in 150-GeV/c $\pi^- p$ interactions in the Fermilab 30-in.-bubble-chamber–proportional-wire-chamber hybrid spectrometer. The dissociations are observed as recoil systems opposite leading particles, the signals of which are separated from background where appropriate by a variant of the Van Hove sector cut, thus allowing the high-mass portion of the spectrum to be observed. Pion dissociation has a cross section of 1758 ± 105 μb, divided among two-, four-, and six-prong events; some ρ^0 production is seen and comes primarily from the $\pi^- \to 2\pi^- \pi^+$ channel. The proton dissociation cross section is 1726 ± 100 μb, again divided among two-, four-, and six-prong events. The final state contains a neutron more frequently than a proton in the two- and six-prong events, a proton more frequently in the four-prong events. Production of Δ^{++} is observed in the $p \to p\pi^+\pi^-$ dissociations.

I. INTRODUCTION

Diffraction dissociation of hadrons, in which they break up into their virtual constituents by transferring four-momentum to other particles, has been one of the main areas of study in high-energy physics for the past several years. It was pointed out by Good and Walker[1] in 1960 that

such a process should occur and that it would be recognized by observing interactions in which either the beam or target particle left the interaction with no change in quantum numbers and relatively small momentum transfer. The dissociation process has been most thoroughly studied in the range of beam momenta from ~10 to 30 GeV/c, and in this region the so-called leading-particle signals are not sharp enough to allow a clean separation of beam dissociation, target dissociation, and other processes. This problem exists because the masses into which hadrons dissociate are not negligible compared to the total energies available at such momenta. The resulting leading-particle signals are mixed with distributions from other processes, perhaps even interfering with them.

It is of importance to extend the studies of the dissociation phenomenon to the Fermilab energy range of roughly an order of magnitude greater beam momentum. In this region the beam and target dissociations are quite clearly separated from each other in kinematic quantities and are usually separated from other processes as well.

This paper presents a systematic study of the dissociations of both the beam and target in interactions of 150-GeV/c π^- mesons with protons. Our aim is to measure not only the leading-particle or diffractive cross sections, but also the dynamic correlations among the dissociation products. Since good multiparticle sensitivity is required for both very fast and very slow particles, a visual detector is essential, and as the cross sections for dissociation are in the mb range, a bubble chamber is the natural one to use. This experiment was performed in the Fermilab 30-in.-liquid-hydrogen-bubble-chamber–proportional-wire-chamber hybrid system. The greatly improved momentum resolution and rudimentary γ-ray detection of the hybrid facility are important factors in obtaining the results presented.

Section II contains a review of the apparatus and exposure. The details of the extraction of diffractive events from leading-particle signals are presented in Sec. III for beam and in Sec. IV for target breakup. The properties of the two dissociations are presented in Sec. V and VI and a summary and discussion are given in Sec. VII.

It is now generally felt[2] that diffractive processes can occur in this energy range in more complex events than those represented by single leading particles. However, in this report we discuss only this more straightforward case. Preliminary results on this topic have been published previously in Refs. 3–5.

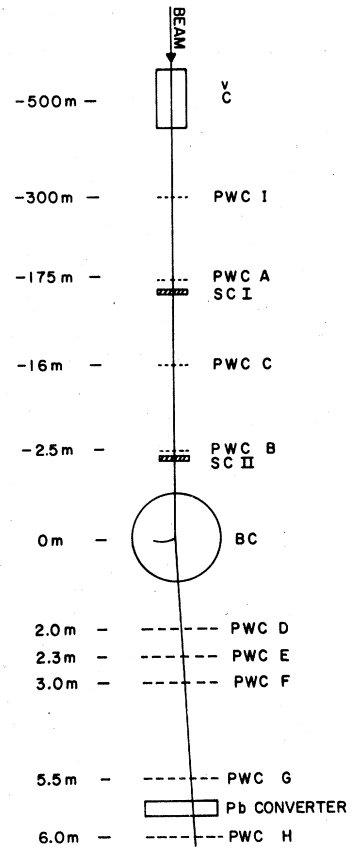

FIG. 1. Schematic layout of the 30-in.-bubble-chamber–proportional-wire-chamber hybrid system.

II. EXPERIMENTAL DETAILS

The apparatus of the Fermilab proportional hybrid system has been discussed in detail elsewhere,[3] and only a brief review is presented here. Figure 1 is a schematic diagram of the spectrometer showing the upstream beam-tagging system, the 30-in. bubble chamber which provides the multiplicity distribution and momentum determination on slow tracks, and the downstream system which provides improved momentum resolution on the fast tracks. Essentially all leading beamlike particles pass through proportional wire chambers (PWC's) D, E, F, and G, and are measured with a momentum resolution $\delta p/p$ of 0.06p%, p measured in GeV/c. Thus leading pions are measured at 150 GeV/c to 9% compared with >50% in the bubble chamber alone. In general, one or more charged tracks from beam dissociations pass through PWC's D, E, and F and have improved momentum determination.

The Pb converter and PWC H subtend an angle of $\pm 1.5°$ at the center of the bubble chamber and

thus showers in that PWC are produced for γ rays forward of Feynman x of ~0.15, and π^0's, the presumed source of most such γ rays, are detected in the same range with reasonable efficiency. No measurement is made of the γ's observed by this technique, but their presence as indicated by the shower is noted.

The system is run in an untriggered mode, recording upstream and downstream information for every track. When an interaction is found in the bubble chamber the upstream information is used, in conjunction with the known bubble-chamber position relative to the wire planes, to determine which set of electronic information belongs with that event. The data from the downstream planes are then combined with the bubble-chamber measurements to provide the improved momentum values.

The exposure consists of 105 000 bubble-chamber pictures yielding 14 750 events with a sensitivity of 0.61 events/μb. The details of the cross-section determination can be found in Ref. 6. For the purposes of physics analysis a smaller fiducial volume yielding 0.43 events/μb was utilized. The sample was put through two measurement passes yielding complete reconstruction on essentially all of the two- and four-prong events and 94% of the six-prong events. The missing events in this latter category are found to have a significant (~25%) influence on the leading-proton category, and cross sections and distributions have been corrected accordingly. All possible hookups of the electronic and bubble-chamber data have been made.

Kinematic fitting, an important tool in the classification of the events, was performed by SQUAW as modified for ultrarelativistic particles by Day.[7] This modification solves the numerical problems associated with very-high-energy particles, but not the possible physical one of events with neutral particles making acceptable fits as if those particles were not present. There is also difficulty in establishing error matrices from the complete hybrid apparatus in so proper a manner as in traditional bubble-chamber experiments. A more complete discussion of the fitting systematics can be found in Ref. 4.

The best evidence that we have been successful in selecting a proper fitted-event sample is given in Fig. 2 which shows a scatter plot of the square of the missing mass versus the transverse-momentum imbalance, and projections, for the four-prong event sample under the assumption that the positive particles are proton and π^+ and that both negatives are π^-. A strong concentration is seen in the region where each of these quantities has a low value, and this concentration corresponds to the events fitted as $\pi^- p \to \pi^-\pi^-\pi^+ p$ shown as shaded in the histograms. From examination of the numbers of events present in the vicinity of the χ^2 cutoff we estimate the purity of this fitted sample as >90%.

In Fig. 3 is seen the distribution of the square of the missing mass in the six-prong events under the hypothesis that the positive tracks are a proton and $2\pi^+$ and the negative tracks are $3\pi^-$, three combinations per event. There is again a peak at zero which is fairly well accounted for by the fitted events $\pi^- p \to 3\pi^- 2\pi^+ p$ shown as shaded. Those shaded combinations not in this central region in general represent incorrect proton assignments for events in the central region with the proper assignment. Careful study of this sample indicates that a contamination of 20% cannot be ruled out, a problem which stems chiefly from the fact that only about 4% of the six-prong events apparently belong in the four-constraint (4C) fit category.

The sample obtained of 4C eight-prong events $\pi^- p \to 4\pi^- 3\pi^+ p$ seems consistent with 100% background and we assume that such a process represents only a negligible fraction of our data.

Positive tracks of momentum less than 1.4 GeV/c are determined to be π^+ or proton by observation of ionization in the bubble chamber. The effects of this momentum cut have been examined in detail[8]; the cut affects the leading-proton region minimally. In events making 4C fits, proton interpretations are used for tracks so assigned by the fits even if the momenta are above the cutoff value. No disagreements have been noted between ionization and fitting in the classification of low momentum tracks as proton or π^+.

III. LEADING-PROTON SIGNALS

In this section we present methods of extracting a sample of π^- beam dissociations by observations of leading-proton signals. Figures 4(a)–4(f) present the distribution of Feynman x, taken as $2P_{\parallel}^*/\sqrt{s}$, for the inelastic two-prong events, the four-prong events broken into the 4C ($2\pi^-\pi^+ p$) and non-4C subsamples, and the six-prong, eight-prong, and ten- through eighteen-prong categories. The separation of two-prong events into elastic and inelastic channels has been discussed elsewhere.[5] The inset in Fig. 4(d) shows the subsample of six-prong events classified as of the 4C fit category $\pi^- p \to 3\pi^- 2\pi^+ p$; the shaded region corresponds to use of a selection procedure for leading protons discussed below. For graphs of 4C fitted events, measured quantities are plotted to facilitate comparisons with nonfitted categories.

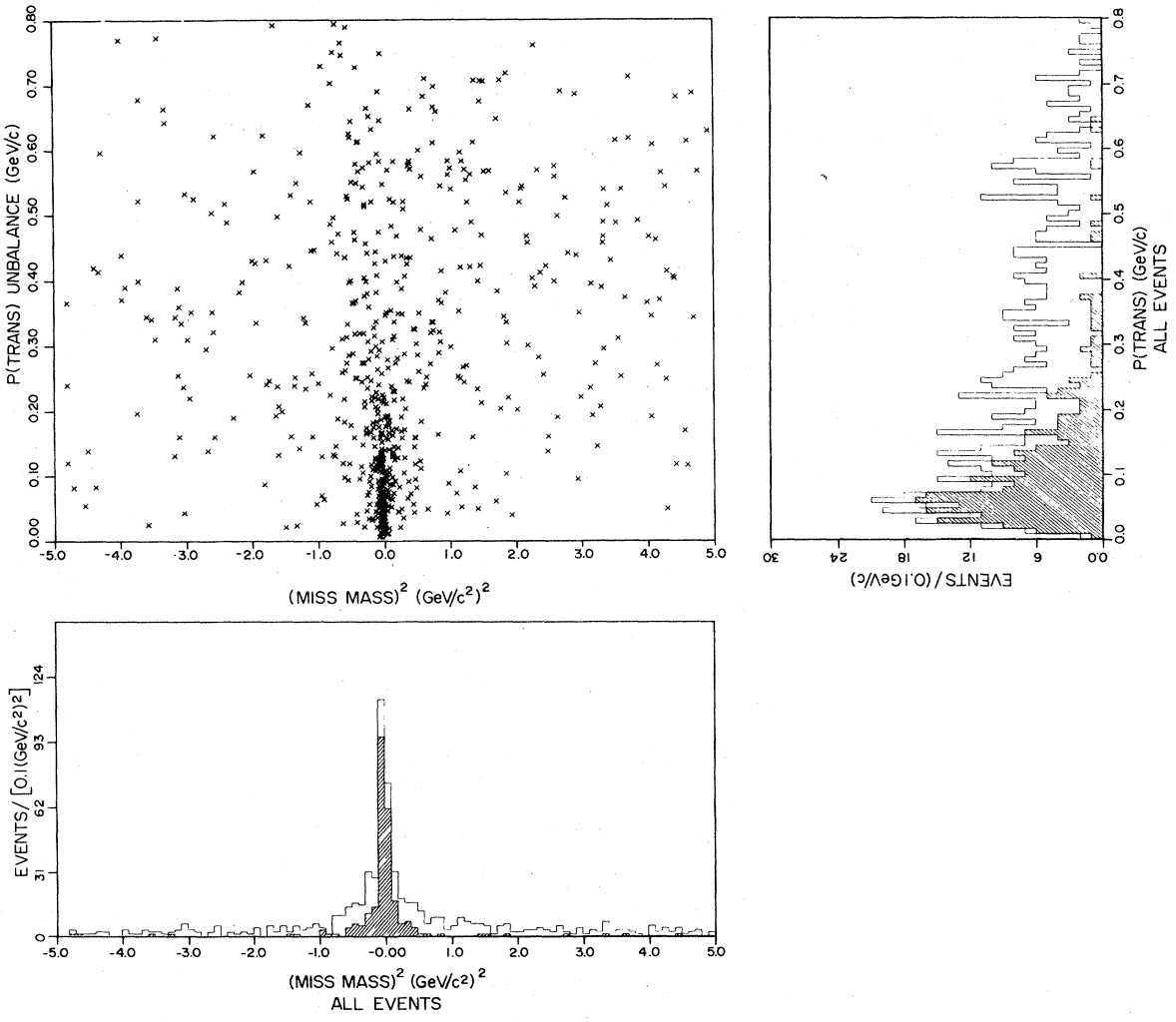

FIG. 2. Scatter plot of the square of the missing mass for the reaction $\pi^- p \to \pi^-\pi^-\pi^+ p$ (MM) versus the transverse-momentum unbalance for all four-prong events, and histograms of the projections of this plot. The shaded regions of the histograms correspond to the reaction $\pi^- p \to \pi^-\pi^-\pi^+ p$ and are seen to be quite clearly separated from the background.

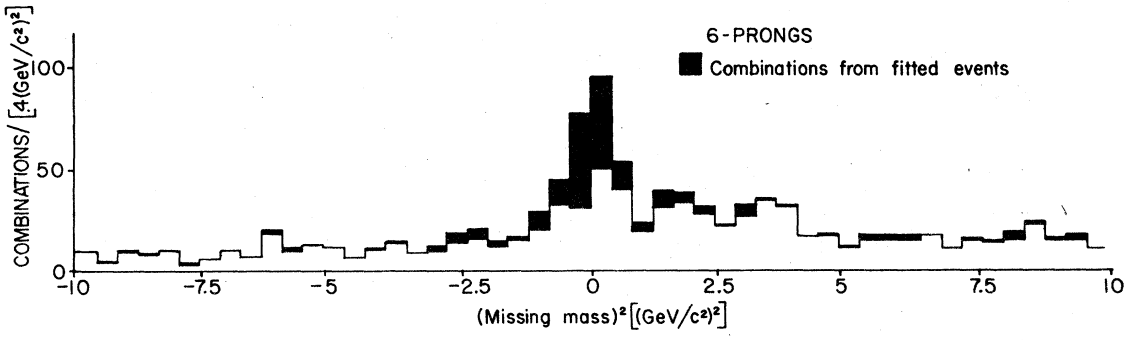

FIG. 3. Distribution in the square of the missing mass for the reaction $\pi^- p \to 3\pi^- 2\pi^+ p$ (MM). The shaded events correspond to the reaction $\pi^- p \to 3\pi^- 2\pi^+ p$.

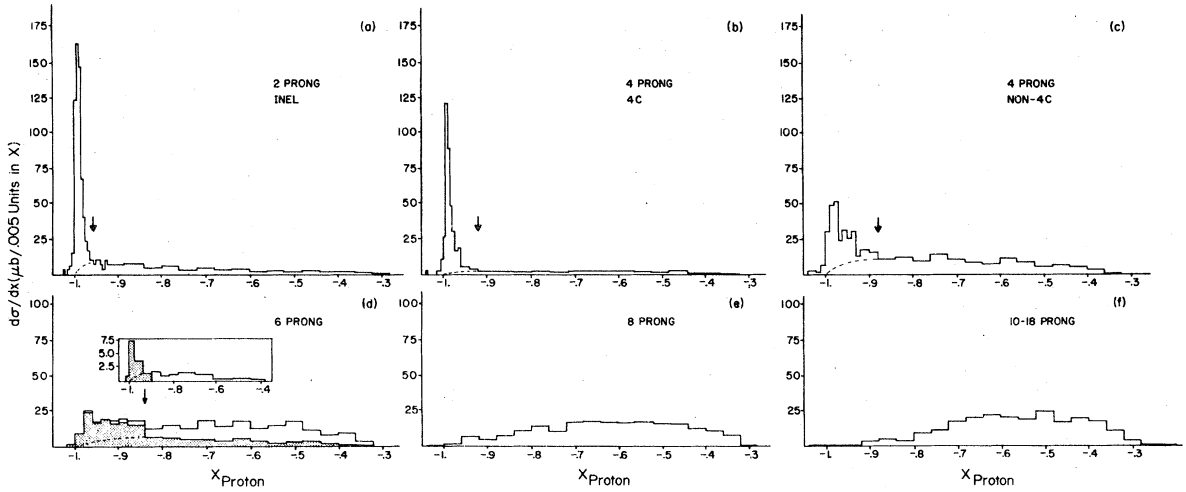

FIG. 4. Feynman-x distributions for protons for (a) the inelastic two-prong events, (b) the four-prong events of the final state $2\pi^-\pi^+p$, (c) the remainder of the four-prong events, (d) the six-prong events, (e) the eight-prong events, and (f) the higher multiplicities. The shaded region in (d) represents the events satisfying the sector cut described in the text. The inset represents the six-prong events of the final state $3\pi^-2\pi^+p$. For fitted-event categories, the measured values of the variable are shown to allow comparison with other channels.

We take the point of view that leading peaks in the vicinity of $x = -1$ correspond to beam-dissociation processes, but that we do not know *a priori* the widths or shapes of these peaks. It is assumed that enhancements above reasonable smooth backgrounds are the signals of interest and in Figs. 4(a)–4(c) such enhancements are seen clearly, the arrows indicating their assumed extent and the dashed curves the estimated backgrounds. In the studies of the properties of diffractive systems, given below and in Figs. 10–15, each event is weighted by the fraction of signal above background for the bin in which it falls in these distributions.

In the six-prong events a small but clear signal is seen in the 4C fit category, while only a distribution inconsistent with reasonable background but lacking any peak is seen in the overall sample. While in the two and four-prong events the leading-proton signals are, as discussed above, quite narrow and reasonably background-free, this is apparently not the case in the non-4C six-prong events. If dissociation of the pion into five charged prongs plus neutrals occurs, it is not unreasonable to expect that the mass of the dissociating system be high, inducing a broad leading-particle peak even at this value of beam momemtum.

The situation is similar to that encountered in lower-energy experiments at much lower dissociation masses, and a similar technique is used to enhance the signal above background. This technique is that of the Van Hove hemisphere cut, the assumption that if the proton truly is leading then no other particle should appear in the backward hemisphere in the c.m. frame. Such a procedure works well for low-mass dissociations but is biased for high masses as it selects a particular region of the dissociation angular distribution.[9] There is also a worry in our case that such a procedure could kinematically select a signal of slow protons which does not correspond to a real physical process. It was felt that a cut made in some plane other than a hemisphere boundary might be more proper here. In Fig. 5

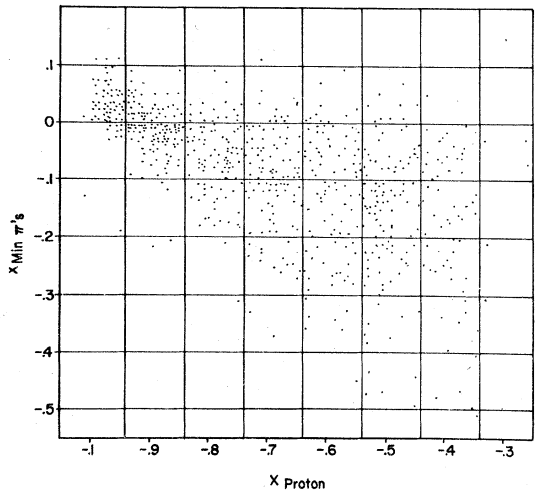

FIG. 5. Scatter plot of the minimum x value for the five fast tracks, assumed pions, in six-prong events versus the x value for the proton.

TABLE I. Leading-proton cross sections.

Channel	Cross section (μb)	Events
2-prong events (inelastic)	570 ± 60	170
4-prong events	848 ± 50	329
$2\pi^-\pi^+p$	392 ± 30	147
Other final states	456 ± 40	182
6-prong events	340 ± 70	120
$3\pi^-2\pi^+p$	22 ± 10	8
Other final states	318 ± 70	112
Total	1758 ± 105	619

is seen a scatter plot of the minimum x value of the five fast tracks of the event, assumed pions, versus the x value for the proton. A concentration is seen in the region $-1.0<x_{\text{proton}}<-0.8$, x_π's >-0.05. A cut at this value for x_π is seen neither to cut strongly into a real leading-proton signal nor to produce one kinematically. As a check on the procedure, an attempt was made to isolate leading-particle signals of both π^+ and π^- in the backward hemisphere using this technique, and no such signal was found.

The shaded region of Fig. 4(d) represents the six-prong data with the restriction that all pions satisfy the criterion $x_\pi>-0.05$. A background curve is indicated as above. No leading-particle signals in the eight-prong or higher-multiplicity samples have been isolated. If such signals are present they are so broad and/or small as to be indistinguishable from background processes.

The cross sections obtained for these various leading-proton signals above background are given in Table I. Corrections of a few percent are made in the non-4C four-prong events and the six-prong events for protons of momentum above the 1.4-GeV/c cutoff. A significant correction for scan inefficiency on very low momentum protons in the two-prong category has been made as in Ref. 5. The results are consistent with others reported from the same experiment[3-5]; any apparent discrepancies are due to different definitions of the leading-particle regions.

IV. LEADING-PION SIGNALS

Extraction of leading-pion signals, corresponding to target dissociation, is hampered by problems of momentum resolution on the fast tracks, a situation not encountered in studying leading protons. The extent of the problem can be understood through comparison of Figs. 6 and 7(b). Each shows the distribution in x for the fast π^- of the 4C fit final state $2\pi^-\pi^+p$; the former in a scatter plot with fitted values used, the latter in a histogram with measured values. In general, of course, high-resolution fitted values are not available, and the peak in Fig. 7(b) serves as a point of comparison in representing data known from the fitted values to have a large component of leading-pion events.

Figure 7(a) shows the distribution in x for π^- from inelastic two-prong events, while Fig. 7(c) shows it for the faster π^- of four-prong events of other than the $2\pi^-\pi^+p$ channel, and Fig. 7(d) for the fastest π^- of six-prong events. A clear though small leading-π^- signal can be seen in the 4C six-prong final state $3\pi^-2\pi^+p$ in the scatter plot of x of the fastest π^- versus x of the proton shown in Fig. 8 using fitted values.

In the inelastic two-prong events the signal though broad is relatively well separated from background. In the 4C event categories clean samples can be separated if fitted values are used. However, for the remainder of the four- and six-prong samples more sophisticated techniques must be employed. There are very few tracks in leading-pion regions in the events of higher multiplicity, and target dissociations of the type under investigation here are assumed to be absent or at least strongly suppressed in those channels.

The discussion above has used a version of the traditional Van Hove cut to separate a leading-proton signal from background in the six-prong events. A similar technique used for leading pions is seen to be quite satisfactory even though the confusion with background results from reso-

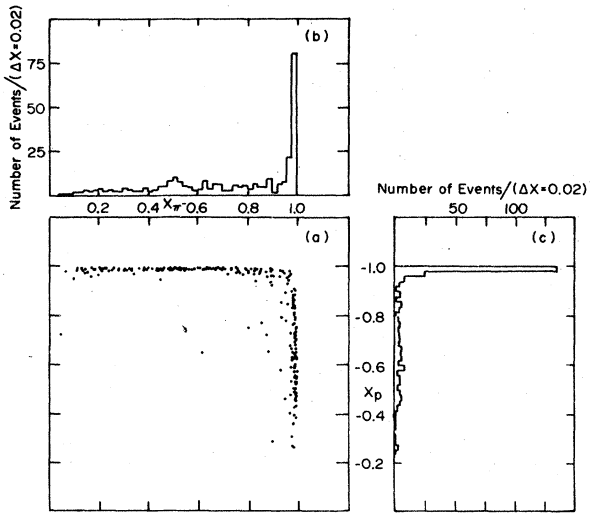

FIG. 6. Scatter plot of the x value for the proton versus the larger of the two x values for the π^- in the $\pi^-\pi^-\pi^+p$ final state. Fitted values are plotted (Ref. 10).

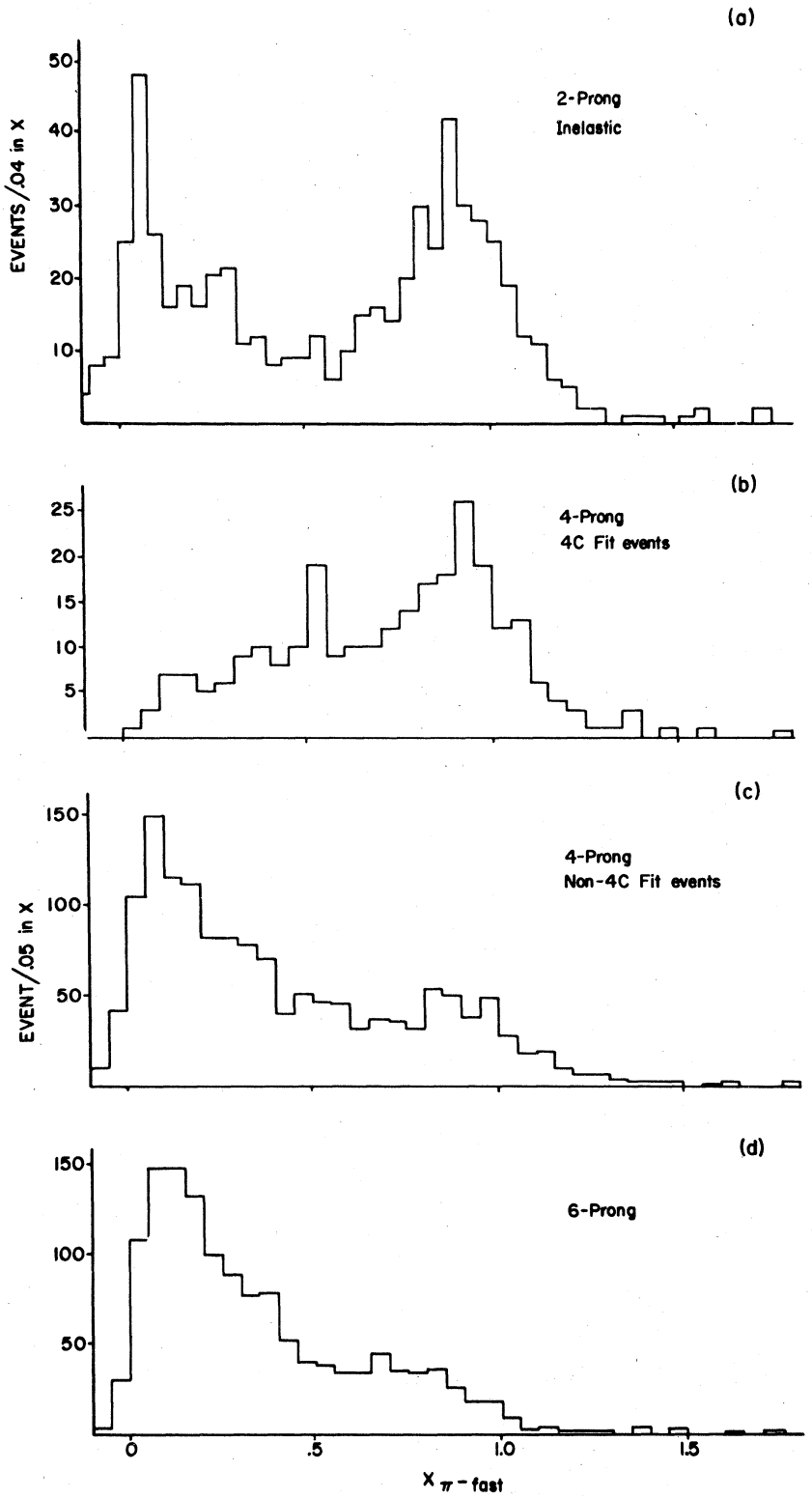

FIG. 7. Feynman-x values for π^-. (a) Inelastic two-prong events, (b) four-prong events of the final state $\pi^-\pi^-\pi^+p$, measured values plotted, only the faster of the two π^-, (c) the remainder of the four-prong events, only the faster of the two π^-, and (d) six-prong events, only the fastest of the three π^-.

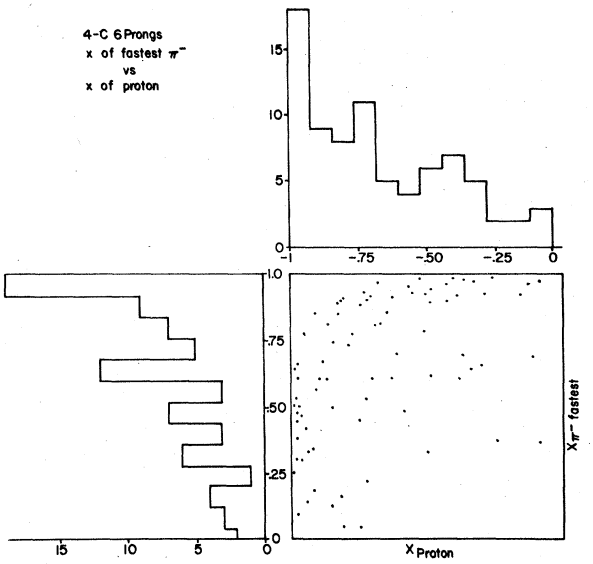

FIG. 8. Scatter plot of the x value for the proton versus the largest of the three x values for the π^- in the $3\pi^-2\pi^+p$ final state. Fitted values are plotted.

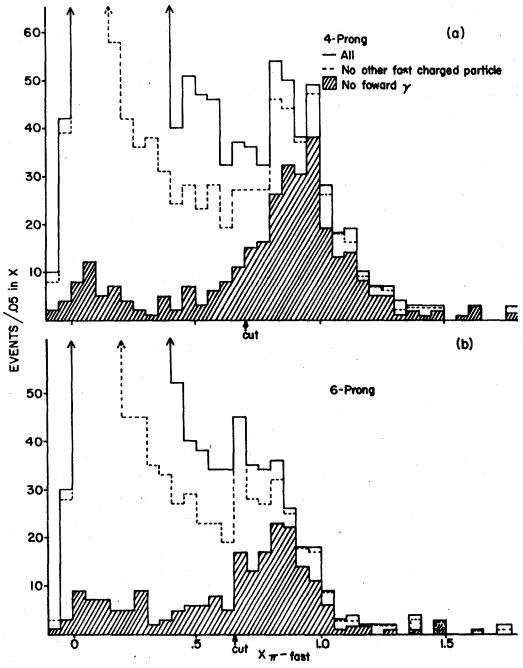

FIG. 9. Demonstration of the enhancement procedure used for the leading pions. The solid curves represent the x_{π^-} distributions for the faster (fastest) π^- of the event. The dotted curves result when events with other fast charged particles are removed. The shaded regions result when fast π^0's, as distinguished by electromagnetic showers in the downstream system, are removed. (a) Four-prong events not of the 4C fit category, (b) six-prong events.

lution effects rather than physical processes. If a pion is truly a leading particle, then there should be no other fast particles in the event. We first make the quite conservative assumption that leading pions should not be accompanied by other tracks with $x > 0.15$. Shown in Fig. 9 are the fast-pion x distributions for the non-4C four-prong and

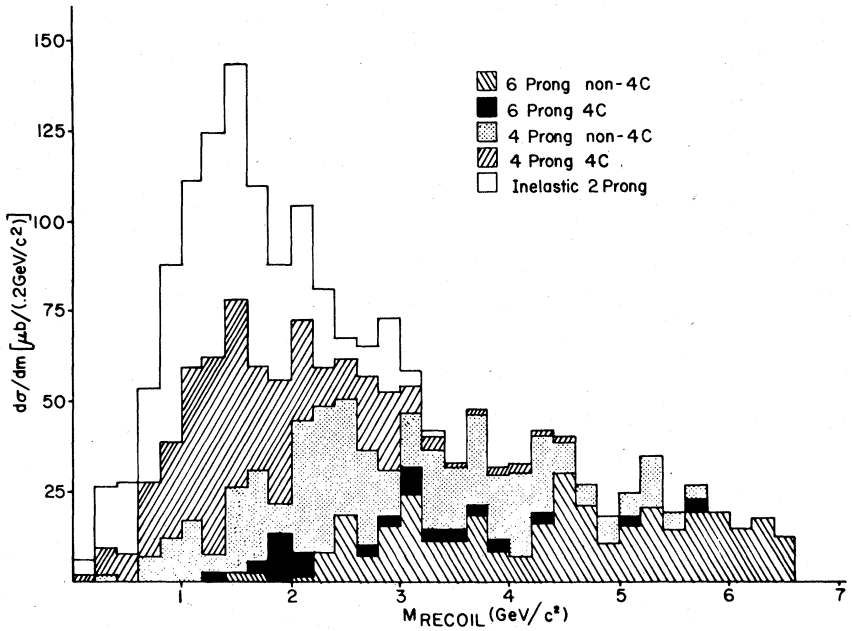

FIG. 10. The pion-dissociation mass spectrum as calculated from the kinematics of the leading recoil protons, the signals of which were extracted above. The different shadings represent different event topologies as indicated in the figure. For events indicated as 4C fits, measured quantities are plotted so that a proper comparison can be made.

TABLE II. Comparison of channel cross sections for pion dissociation. These fractions are calculated assuming equal numbers of produced ($\pi^+\pi^-$) and ($\pi^0\pi^0$) pairs. The observed values are normalized to the 4C four-prong events having the value 0.50.

Channel \ Number of final-state pions	3	5	7	Observed
Inelastic two-prong events	$\frac{1}{2}$	$\frac{1}{4}$	$\frac{1}{8}$	0.73 ±0.10
4C four-prong events	$\frac{1}{2}$			0.50
Non-4C four-prong events		$\frac{1}{2}$	$\frac{3}{8}$	0.58 ±0.07
4C six-prong events		$\frac{1}{4}$		0.056±0.026
Non-4C six-prong events			$\frac{3}{8}$	0.40 ±0.09
4C eight-prong events			$\frac{1}{8}$	~0

all of the six-prong events on an expanded scale. The solid histogram represents all the events, and the dotted one those that remain after this cut; some signal enhancement in the leading-pion region is observed.

If a fast π^- is to be a leading particle, it should also not be accompanied by fast π^0's which are evidenced by showers appearing in the chamber PWC *H*. If showers are defined as >11 wires fired in this chamber, then eliminating them leaves those events represented by the shaded regions in Figs. 9(a) and 9(b). There is a finite probability that true leading pions will interact in the lead converter and produce a shower seen in the *H* chamber. This effect is 7% as determined through studies of beam tracks and leading pions of 4C fitted events. The distributions in Fig. 9 and the cross sections for leading-pion–target-dissociation processes are corrected upward accordingly. The leading-pion signals observed in Figs. 7 and 9 are assumed to represent target-dissociation phenomena, and the particles recoiling against such leading pions are assumed to be the dissociation products. These particles form the contents of Figs. 16–20.

V. PION-DISSOCIATION PHENOMENA

Presented in this section are mass and momentum-transfer distributions as determined from

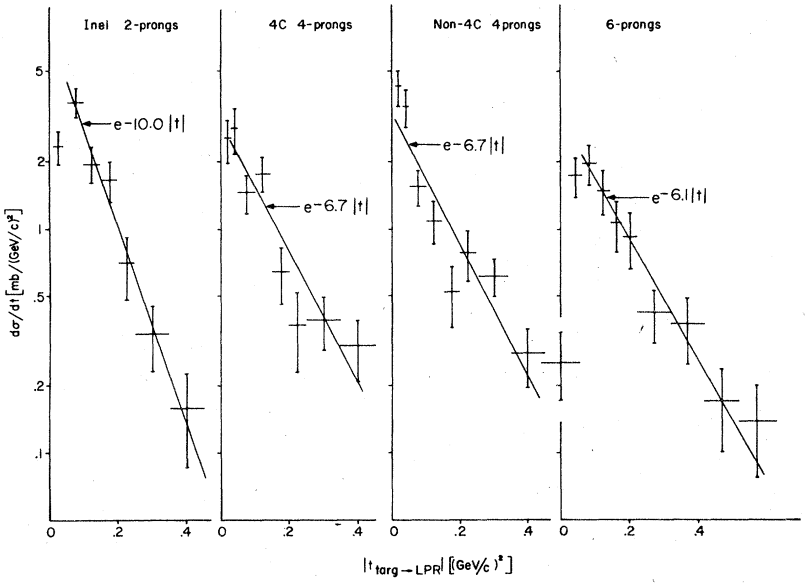

FIG. 11. Momentum-transfer distributions to leading protons. The straight lines represent best fits of the form $e^{-b|t|}$, the fit being made over the regions of t indicated by the lengths of the lines with results for b of 10.0 ± 0.4 (GeV/c)$^{-2}$ for inelastic two-prong events, 6.7 ± 1.0 (GeV/c)$^{-2}$ for each of the four-prong categories separately, and 6.1 ± 0.9 (GeV/c)$^{-2}$ for the six-prong events.

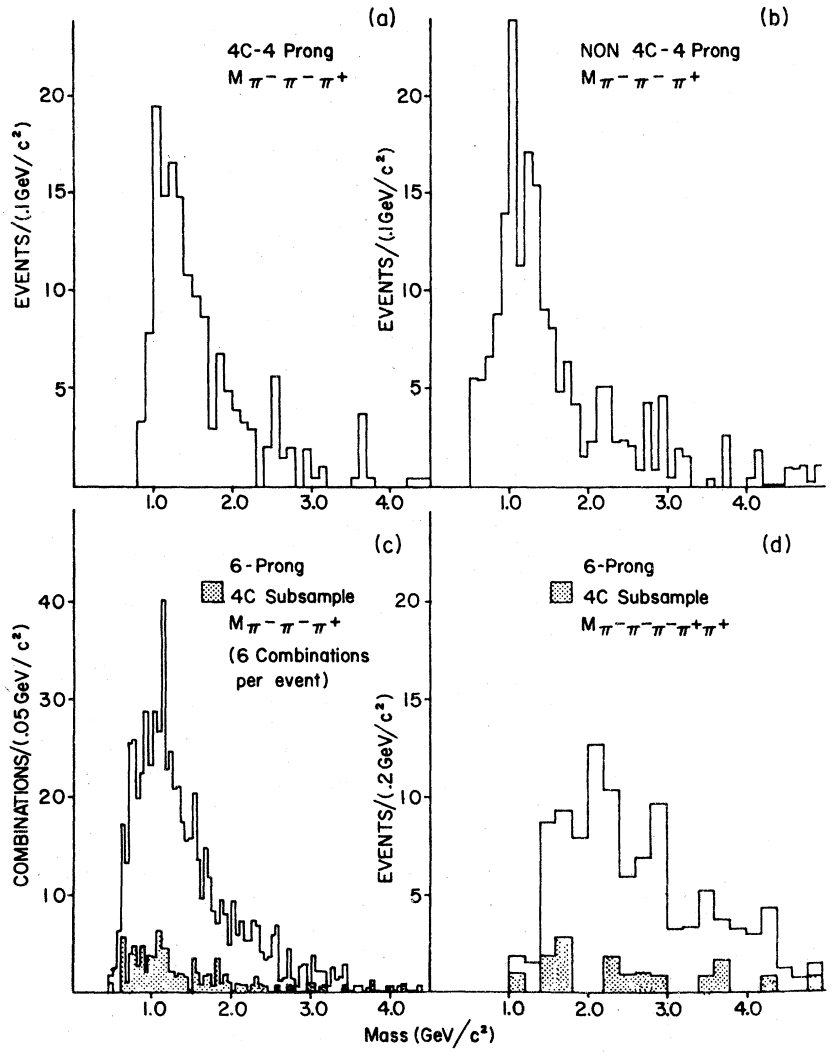

FIG. 12. Three-pion mass distributions for the 4C fit and non-4C four-prong events, and for the six-prong events. Five-pion mass distribution for the six-prong events. All distributions are for pions recoiling against the leading-proton signals extracted above.

the recoil protons, together with submass, angular, and Feynman-x distributions for the dissociation products. It should be kept in mind that although the events of interest are relatively easily separated through use of leading-proton signals, the dissociation products themselves are fast tracks and may in some cases show the effects of limited momentum resolution. Shown in Fig. 10 is a distribution of the masses recoiling from the sum of all the leading-proton signals discussed above. This quantity is based on the measurements of the beam track and slow proton only, and represents a quite accurate picture of the pion dissociation spectrum. It is seen that the inelastic two-prong events and 4C four-prong events concentrate in the region of the well-known A objects. The dissociations into more particles fall at considerably greater masses.

The two major contributions to the A_1 region, taken as $M<1.4$ GeV/c^2 can be compared on this plot. On the assumption that the A_1 has isospin one and decays to $\rho\pi$, equal contributions for the inelastic two-prong sample from

$$A_1^- \to \rho^-\pi^0, \quad \rho^- \to \pi^-\pi^0$$

and for the 4C four-prong sample[10] from

$$A_1^- \to \rho^0\pi^-, \quad \rho^0 \to \pi^+\pi^-$$

are predicted. The value which is obtained from

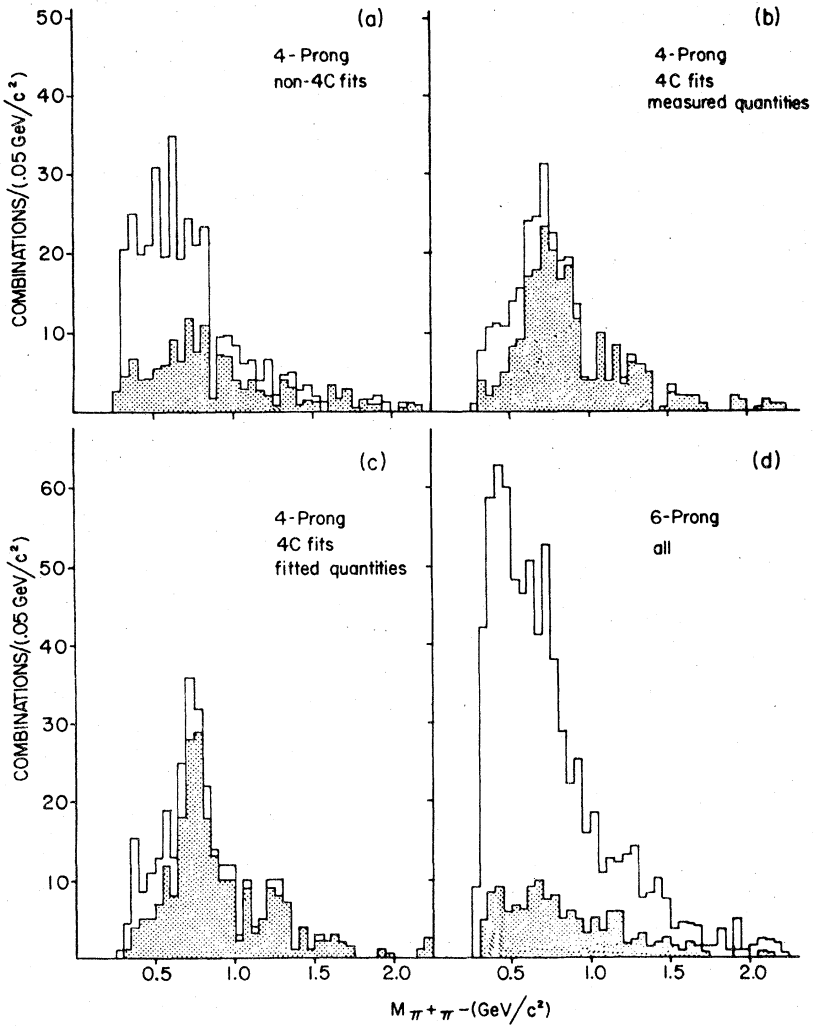

FIG. 13. $\pi^+\pi^-$ mass distributions in the beam-dissociation system. (a) Four-prong non-4C fits, (b) four-prong 4C fits, measured quantities, (c) four-prong 4C fits, fitted quantities, (d) all six-prong events. The shaded regions in the figure represent data with the restriction $y_{\text{lab}}(\pi^+\pi^-) > 4.7$.

the data is

$$\frac{\sigma(\pi^+2\pi^-)}{\sigma(\pi^- + \text{neutrals})} = 0.71 \pm 0.19 ,$$

where some systematic uncertainty is included in the error. This is consistent with the prediction above only if $(29 \pm 19)\%$ of the inelastic two-prong events with beam-dissociation mass in the A_1 region represent some process other than actual A_1 production. Other differences between the two- and four-prong data samples are discussed below.

A general feature of the pion dissociations is that there seems to be a marked preference for neutral rather than charged pions in the decay products. Assuming G-parity conservation, the final state will in general consist of a single π^- and a number of pion pairs which may be either $(\pi^+\pi^-)$ or $(\pi^0\pi^0)$. The $(\pi^+\pi^-)$ pairs can result from decay of ρ^0 mesons while the $(\pi^0\pi^0)$ pairs cannot, and there is no obvious source which favors the neutral over the charged pairs. Thus making the conservative assumption that the probabilities of producing charged and neutral pairs are equal, the channel cross-section ratios are obtained in Table II for three, five, and seven final-state pions. No mixture of these ratios is in agreement with the data for any mass region, there always being too many missing-neutral-type events.

The momentum-transfer distributions to the leading protons in the inelastic two-prong, 4C and non-4C four-prong, and six-prong data samples are shown in Fig. 11. The straight lines in the figure indicate best fits of the form $e^{-b|t|}$,

with b values indicated. The significant difference observed between the inelastic two-prong sample and the $2\pi^-\pi^+p$ final state is further evidence that the two types of reactions are not simply different I-spin manifestations of the same process.

In Fig. 12 are presented three- and five-pion mass distributions for the events under discussion. In the 4C four-prong sample this distribution is the same as that for the mass recoiling from the leading proton, differing only because measured rather than fitted values are shown. It is interesting to note that although the recoil mass differs markedly between the 4C and non-4C four-prong events, the mass observed in the charged particles appears to be the same for the two categories. In the case of the six-prong events the three-pion mass peaks at values as low as in the four-prong events while the five-pion mass peaks somewhat higher, but is nonetheless distributed at much lower values than is the recoil mass.

The $\pi^+\pi^-$ distributions are presented in Fig. 13 and give an indication of the amount of ρ^0 production present in these pion dissociations. In all cases the shaded region of the histogram is that subset of the data satisfying the relation $y_{1ab}(\pi^+\pi^-) > 4.7$, a cut which is seen to enhance somewhat the ρ^0 signal in the $2\pi^-\pi^+p$ final state when fitted quantities are plotted [Fig. 13(c)]. While there are weak indications of signals above hand-down backgrounds in the non-4C four-prong and six-prong samples, the dominant one occurs in the 4C four-prong data. Note that this topological dependence of the ρ^0 cross section in beam dissociations differs markedly from that of the inclusive ρ^0 signal[11] where there are 0.21 ρ^0's/event in the four-prong data and roughly twice this number in all higher multiplicities. Figure 13(b) shows the 4C data plotted with measured quantities. Resolution effects broaden the observed peak somewhat, but are not serious enough to cause a clear signal to be missed.

An attempt has been made to determine possible spin parities of the dissociating system through observation of some of the standard angular distributions. As these are particularly susceptible to resolution effects, they are presented only for the 4C four-prong events and only with fitted quantities. The distribution of the direction of the three-pion "decay plane" normal in the Jackson frame is shown in Fig. 14(a), folded about zero to account for the two identical π^-. The data are presented separately for the 3π mass region below 1.4 GeV/c^2, for an intermediate mass region extending to 1.9 GeV/c^2, and for the higher masses. The distribution in the low-mass or A_1 region seems consistent with a $\sin^2\Theta$ form, as expected for the usual 1^+ assignment of the A_1. The intermediate mass region is also in reasonable agreement with this form, while the events at higher masses indicate dominance of other spin values.

The Jackson angle of ρ^0 mesons is shown in Fig. 14(b) for the restriction $0.67 < M_{\pi^+\pi^-} < 0.87$ GeV/c^2 as the definition of the ρ region. This plot shows serious disagreement with the usual picture of a 1^+ A_1 decaying via s wave to ρ and π mesons, which predicts a flat distribution in this angle. If the cut requiring fast pion pairs is made

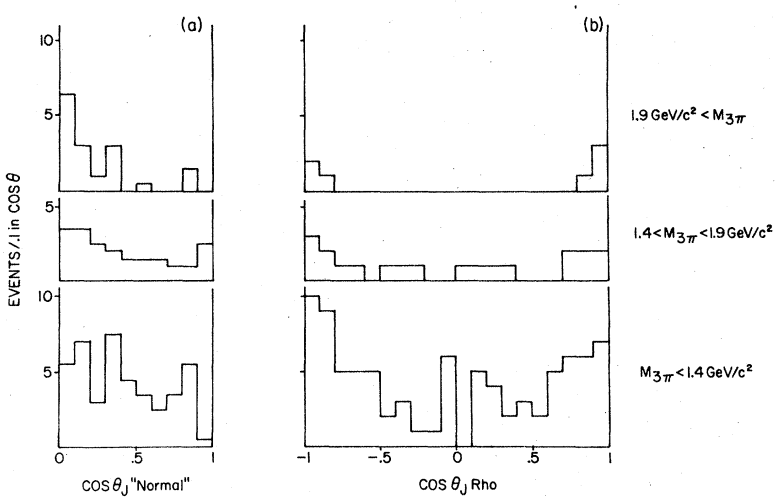

FIG. 14. Angular distributions in the Jackson frame for pion dissociation into $2\pi^-\pi^+$. (a) For the three-pion decay plane normal, distribution folded about zero, (b) for ρ^0 mesons defined by $0.67 < M_{\pi^+\pi^-} < 0.87$ GeV/c^2. Histograms are presented for different regions of three-pion mass as indicated. These data are calculated with fitted values in the beam dissociation $2\pi^-\pi^+p$ final state.

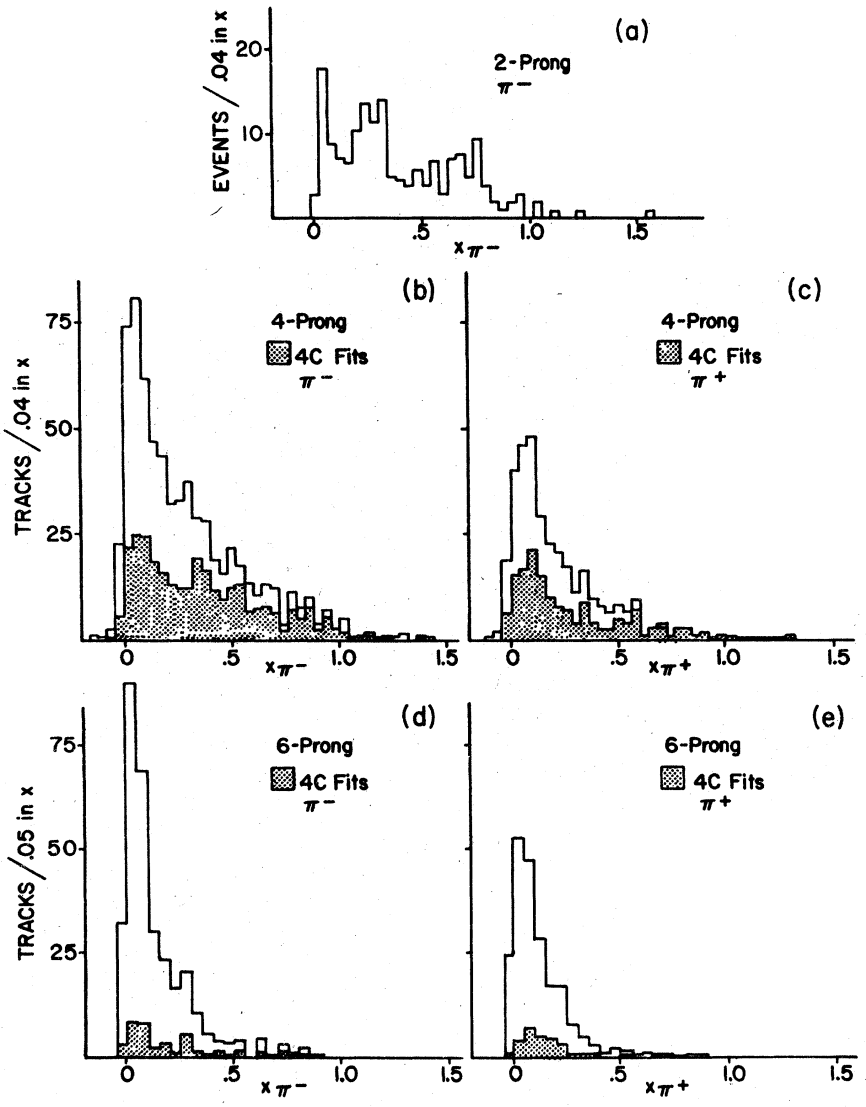

FIG. 15. Distributions in Feynman x for the π^- and π^+ beam-dissociation products with different topologies as indicated in the figure. The structure observed for the two-prong events is not well understood.

to enhance the ρ signal above background, the backward peak is eliminated and a reasonably flat distribution plus the forward peak remains. The true distribution in this quantity may be asymmetric.

Finally we show in Fig. 15 the Feynman-x values for the dissociation product pions for the two-, four-, and six-prong event categories. Two features are noted: The first is that the distribution in the two-prong events has a peak near zero, typical of the other categories, and another enhancement extending from 0.18–0.35 in x. Such a distribution cannot be produced for a pion resulting from $A_1^- \to \rho^-\pi^0 \to \pi^-\pi^0\pi^0$ decay and represents further indication of other processes. Otherwise all the distributions do peak quite strongly near $x = 0$, which is the usual region of multiparticle production in nondiffractive events.

VI. PROTON-DISSOCIATION PHENOMENA

The proton-dissociation sample, i.e., those particles recoiling from the leading pions, is not expected to be so clean as is the beam-dissociation sample selected from the leading protons. However, once a sample is selected the studies which can be performed are more complete and straightforward than in the beam-dissociation case. The target fragments are slow in the laboratory and thus allow proton versus π^+ identification for the majority of the events. It is also

possible to make mass plots and angular distributions even for unfitted events without problems from resolution effects.

The momentum accuracy for the leading pions is not sufficient to allow a meaningful calculation of the mass recoiling from such a particle, and for mass distributions we are thus limited to calculations involving the observed fragments only. Momentum transfers to leading pions do seem to lead to meaningful results with an estimated resolution of 18%. Such distributions are shown in Fig. 16 for the same categories of events as discussed above, namely the inelastic two-prong events, the four-prong events of the $2\pi^-\pi^+p$ final state, the remainder of the four-prong events, and the six-prong events. All are fitted to the $e^{-b|t|}$ form with results indicated. As in the case of the beam dissociations, the distribution seems to be somewhat steeper in the two-prong events than in the other classes. In this case the two-prong events can come from the processes $p \to p\pi^0$ and $p \to n\pi^+$ which have no counterpart in the higher-multiplicity events. When the two-prong data are fitted in the limited range of $0 < |t| < 0.45$ $(\mathrm{GeV}/c)^2$ a steeper slope of 8.1 ± 1.1 $(\mathrm{GeV}/c)^{-2}$ is obtained,[5] and results in a more satisfactory fit.

The target-breakup data fall naturally into categories of events with and without observed protons, those without protons being referred to as neutron events in the following. In the four- and six-prong cases the cut on proton momentum incorrectly classifies a significant number of events and a correction must be made separately for each channel; the cross sections are quoted in Table III both with and without this correction. The ratios of proton to neutron cross sections after corrections are given for the two-, four-, and six-prong events by the values 0.76 ± 0.10, 1.89 ± 0.34, and 0.71 ± 0.18. The two- and six-prong values are in good agreement with each other and are near the value 0.5 expected if all the nucleons come from decay of $I = \frac{1}{2}$ objects. The four-prong events differ markedly from the others and from this simple prediction. However, as will be seen, the $p\pi^+\pi^-$ dissociations seen in the 4C four-prong final state proceed predominantly through Δ^{++} formation while the other channels show relatively little evidence of this resonance. Thus it seems that the $p\pi^+\pi^-$ category represents special events, and if they are removed from the four-prong sample the proton-to-neutron ratio becomes 0.96 ± 0.21, a 1-standard-deviation difference from the two- and six-prong samples,

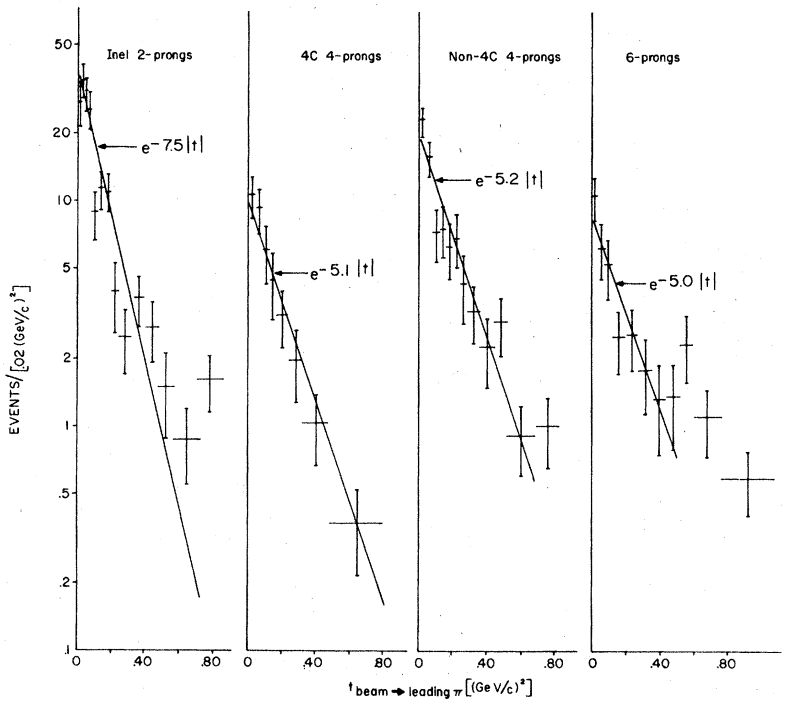

FIG. 16. Momentum-transfer distributions to leading pions. The straight lines represent best fits of the form $e^{-b|t|}$, the fit being made over the regions of t indicated by the lengths of the lines. The values of b are determined to be 7.5 ± 1.0 $(\mathrm{GeV}/c)^{-2}$ for the inelastic two-prong events, 5.1 ± 1.0 $(\mathrm{GeV}/c)^{-2}$ for the 4C four-prong events, 5.2 ± 0.6 $(\mathrm{GeV}/c)^{-2}$ for the non-4C four-prong events, and 5.0 ± 1.1 $(\mathrm{GeV}/c)^{-2}$ for the six-prong events.

TABLE III. p^* cross sections in μb. For comparison: Elastic cross section = 3240 ± 150 μb; inelastic cross section = 21 000 ± 280 μb.

2-prong events		
$\pi^- p \to \pi^- p^*$ all 2-prong events	720 ± 50	
$\pi^- p \to \pi^- p^*$ $\searrow p + X^0$	310 ± 30	
$\pi^- p \to \pi^- p^*$ $\searrow \pi^+ + X^0$	410 ± 40	
4-prong events	**Raw data**	**Corrected for unobserved protons**
$\pi^- p \to \pi^- p^*$ all 4-prong events	722 ± 80	
$\pi^- p \to \pi^- p^*$ $\searrow \pi^+ \pi^- p$	232 ± 23	
$\pi^- p \to \pi^- p^*$ $\searrow \pi^+ \pi^- p X^0$	204 ± 30	240 ± 37
Sum of two above, all 4-prong proton events	436 ± 42	472 ± 44
$\pi^- p \to \pi^- p^*$ $\searrow \pi^+ \pi^+ \pi^- X^0$	286 ± 39	250 ± 39
6-prong events		
$\pi^- p \to \pi^- p^*$ all 6-prong events	284 ± 38	
$\pi^- p \to \pi^- p^*$ $\searrow \pi^+ \pi^+ \pi^- \pi^- p$	31 ± 10	
$\pi^- p \to \pi^- p^*$ $\searrow \pi^+ \pi^+ \pi^- \pi^- p X^0$	75 ± 16	87 ± 18
Sum of two above, all 6-prong proton events	106 ± 20	118 ± 22
$\pi^- p \to \pi^- p^*$ $\searrow \pi^+ \pi^+ \pi^+ \pi^- \pi^- X^0$	178 ± 28	166 ± 28

2.2 standard deviations from the $I = \frac{1}{2}$ value.

The mass distributions for the charged particles in the four- and six-prong events are shown in Figs. 17(a) and 17(c) for the cases where a proton is observed. Figure 17(b) shows for comparison the three-body $p\pi^+\pi^-$ mass observed in the six-prong events. The charged mass represents the full proton-dissociation mass distribution in the 4C fit events and a lower limit to the true distribution for the remainder. Yet in the observed distribution the 4C four-prong events peak at the lower masses indicating that this class of events is quite different.

The data on Δ^{++} production are contained in Fig. 18(a) for the four-prong events and Fig. 18(b) for the six-prong events. Although there are probably a few Δ^{++} events in the other channels, clearly the bulk of them is associated with the $p \to p\pi^+\pi^-$ process which, furthermore, they dominate. As in the case of the ρ^0, the topological dependence of the Δ^{++} cross section in target dissociations differs from the inclusive behavior[8] where production at the level of 400 μb is observed in each of the four-, six-, eight-, and ten-prong categories. A possible Δ^0 signal is seen in Fig. 18(c) which presents the $p\pi^-$ mass in the 4C four-prong events.

Angular distributions for the 4C fit events are shown in Fig. 19. The cosine of the Jackson angle is presented for the "decay plane" normal, the Δ^{++}, and the protons. As in the beam-dissociation case, the distributions are presented separately for the low, medium, and high regions of $p\pi^+\pi^-$ mass. That for the normal is almost flat at low masses and peaks progressively more strongly at zero for increased values. For intermediate $p\pi^+\pi^-$ masses the distribution of the Δ's shows some asymmetry. The process apparently proceeds with relatively low angular momentum, with values and interference effects increasing with $p\pi^+\pi^-$ mass.

The distribution of the Jackson angle for the protons is interesting. Those from higher $p\pi^+\pi^-$ masses peak sharply along the direction of the target incident in the $p\pi^+\pi^-$ rest frame, and since this peaking is so pronounced, a fact also observed in the non-4C and six-prong events, it is useful to examine longitudinal momenta in the

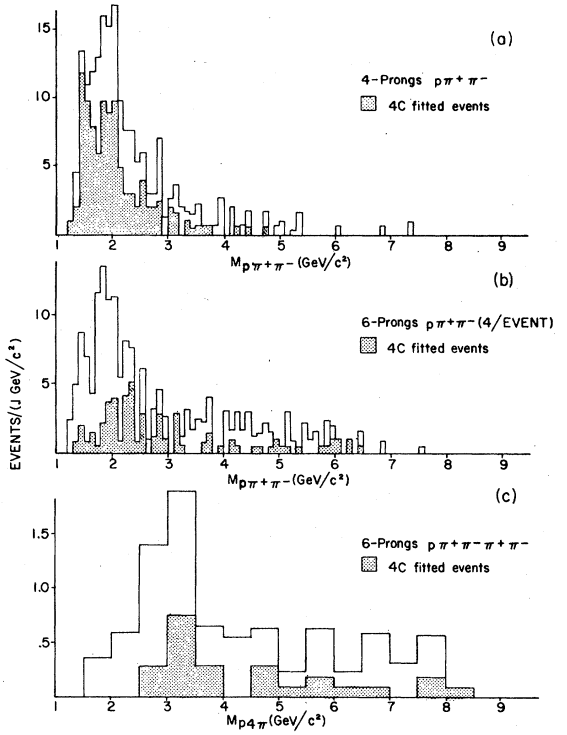

FIG. 17. Charged-particle mass distributions for target dissociations with observed protons. (a) $p\pi^+\pi^-$ distributions in four-prong events, (b) $p\pi^+\pi^-$ distributions for six-prong events, (c) $p2\pi^+2\pi^-$ distributions for six-prong events. In all cases the proton and pions are part of the system recoiling from the leading beamlike π^-.

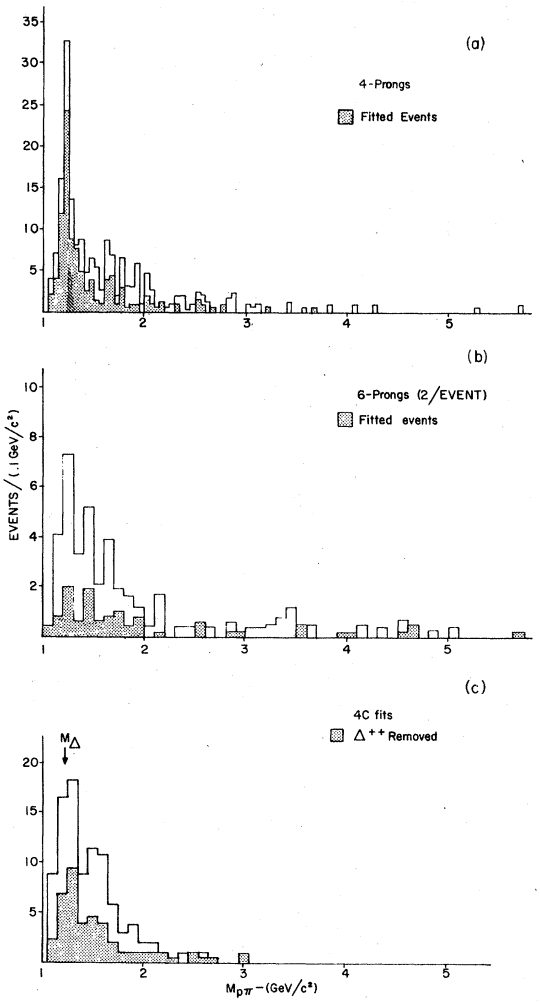

FIG. 18. Proton-pion mass distributions in target-dissociation samples. (a) $p\pi^+$ mass for the four-prong events, (b) $p\pi^+$ mass for the six-prong events. The shaded regions of the histograms represent the 4C fit cases. A clear Δ^{++} signal is observed in the 4C four-prong channel, (c) $p\pi^-$ mass for the 4C four-prong events. The shaded region represents those events remaining when the Δ^{++} signal ($1.14 < M_{p\pi^+} < 1.34$ GeV/c^2) is removed. In all cases the proton and pion are part of the system recoiling against the leading beamlike π^-.

Jackson frame instead of polar angles. To do this we define the variable x_l, an analog of Feynman x, but in the rest frame of the lower vertex particles instead of the overall c.m. system:

$$x_{l \text{ for proton}} = \frac{-\vec{p}_{\text{proton}} \cdot \hat{p}_{\text{target}}}{p_{\text{proton, max}}} \quad \text{in rest frame of slow charged particles.}$$

An apparent leading peak in this quantity might indicate double Pomeron exchange or some similar large momentum gap phenomenon. The distributions in x_l for the four- and six-prong categories of events are shown in Fig. 20. Note that for non-4C events there is an effective cutoff near zero induced by the proton laboratory-momentum limit of 1.4 GeV/c. There is apparently peaking in the extreme backward direction for the four-prong non-4C events and there may be an additional source of protons in this case different from that of the other categories.

VII. SUMMARY AND DISCUSSION

We have observed strong leading-particle signals in the distributions of Feynman x of both final-state protons and π^- in $\pi^- p$ interactions at 150 GeV/c. The observation of the beamlike leading-pion signal is made possible through the improved momentum resolution provided by downstream PWC's of a hybrid system.

Beam dissociation is observed in inelastic two-prong events, and in four- and six-prong events each of which can be divided into 4C fit (no missing neutrals) and non-4C subsamples. The beam-dissociation mass spectrum extends from threshold to ~6.5 GeV/c^2 as observed by the leading-particle technique. The cross section is

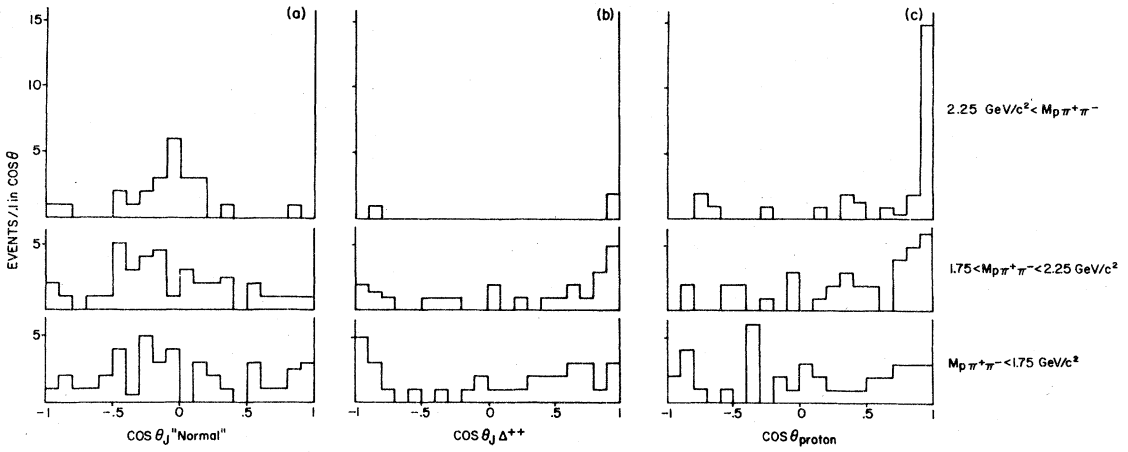

FIG. 19. Angular distributions in the Jackson frame for proton dissociation into $p\pi^+\pi^-$. (a) The decay plane normal, (b) the Δ^{++} objects defined as $1.14<M_{p\pi^+}<1.34$ GeV/c^2, (c) the protons. To avoid biases due to the p_{1ab} cut, the protons are presented only for the 4C fit four-prong events, and are plotted with fitted values. Histograms are presented for different regions of $p\pi^+\pi^-$ mass as indicated.

found to be 1758 ± 105 μb. The larger mass values are seen predominantly in the higher-multiplicity events and represent observation of processes inaccessible at beam momenta of less than 30 GeV/c.

These data seem to consist of four separate types of events. The first is the usual production of what is loosely referred to as A mesons with decay to $\rho\pi$. It encompasses essentially all of the beam-dissociation 4C four-prong data and roughly 70% of the inelastic two-prong data.

By I-spin invariance there should be equal amounts of A production in the two-prong and 4C four-prong categories, with identical momentum-transfer distributions to the recoil protons in the two cases. These facts taken together indicate the presence of a second component in the two-prong sample produced with low momentum transfer and with no counterpart in the 4C four-prong events. This signal, which is 30% of the two-prong sample, exists statistically at a 2.4-standard-deviation level for the entire sample, or a 1.5-standard-deviation level for masses less than 1.4 GeV/c^2. The possibility that such a signal represents misclassified elastic scattering events cannot automatically be ruled out. It is indicated in Ref. 5 that such a contamination of the inelastic two-prong sample has an upper limit of 5%, a value which is not in disagreement with the excess in leading-proton two-prong events over 4C four-prong events. If on the other hand this excess represents a real effect, it could result from an interference between amplitudes of I spins of zero and two, or from production of a final state involving η^0 mesons with their neutral decay. In the latter case the corresponding charged η^0 decays would form part of the four-prong non-4C fit category where they are not inconsistent with the cross section or t distribution observed.

A third component involves the beam dissociating into five pions such as that observed in $\pi^- d$ coherent reactions at 15 GeV/c.[12] However, this is seen to be a minor fraction of the total, witness the small cross section in the 4C six prong events. Finally there is production of high-mass dis-

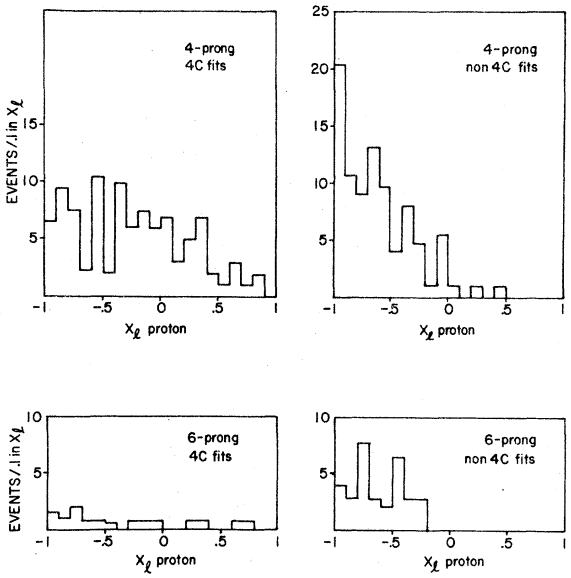

FIG. 20. Distributions in the lower vertex x value x_l, defined in the text, for the protons of target-breakup four- and six-prong events. Events with the value $x_l = -1$ have an outgoing proton carrying all the momentum of the incident target, as evaluated in the rest frame of the slow charged particles recoiling against a leading pion.

sociations, a component with neutrals essentially always present. A possible explanation is that it contains a significant fraction of states such as $\omega^0+\rho^-+$pions. The presence of the ω^0 guarantees that there be no 4C-fit events of any type and also provides a source of the very-low-mass $\pi^+\pi^-$ pairs seen in Figs. 13(a) and 13(c).

Target dissociations are observed via leading pions and, as such, are not a sample so cleanly separated from background as are the beam dissociations. Keeping in mind this limitation, the remainder of the study is better performed with target than beam dissociations. The separation of most of the positive tracks into π^+ or proton adds a new dimension to the results. It would be interesting to see a followup to this experiment involving pp collisions. The leading slow proton signals could be used to obtain cross sections and recoil-mass and momentum-transfer distributions, and with a knowledge of these, a clean target-dissociation sample selected on which to study dynamic correlations.

The chief features of proton dissociation observed are the relatively broad distribution of masses obtained and the limited multiplicty range of two- through six-prong events. The cross section obtained of 1726 ± 100 μb is essentially the same as that for pion dissociations. Neutron production is preferred over protons by an amount near that predicted from $I=\frac{1}{2}$ considerations for the two- and six-prong categories. In the four-prong events, where the 4C category proceeds predominantly through Δ^{++} production, protons dominate the final state. The only strong Δ^{++} signal observed is indeed that in this channel, where some Δ^0 may also be visible.

The most striking feature of the angular distributions is that the outgoing protons maintain the direction of the target in the rest frame of the slow charged particles. In the non-4C four-prong events this effect is particularly pronounced.

ACKNOWLEDGMENTS

We wish to thank the staffs of our several institutions for their work in scanning the film and completing two measurement passes. We also wish to thank the Fermilab neutrino section for aid given us during the setup and running periods. One of us (J.E.B.) would like to thank the Fannie and John Hertz Foundation for financial support and another (P.W.L.) the Johns Hopkins University for support during much of this work and Professor W. D. Walker for many helpful discussions. This effort was supported in part by the United States Department of Energy and the National Science Foundation.

---

*Present address: DESY, Hamburg, West Germany.
†Present address: New England Nuclear Corporation, Billerica, Mass.
§Present address: Polytechnic Institute of New York, Brooklyn, N.Y.
||Present address: Indiana University, Bloomington, Indiana.
¶Present address: Purdue University, West Lafayette, Indiana.
**Present address: Argonne National Laboratory, Argonne, Illinois.
††Present address: Dialog Systems, Inc., Belmont, Mass.
‡‡On leave of absence from Tel-Aviv University, Israel.
§§Present address: SLAC, Stanford, California.
||||Present address: Tel-Aviv University, Israel.
¶¶Present address: Weizmann Institute of Science, Rehovot, Israel.
***Present address: Tufts University, Medford, Mass.
†††Present address: Rockefeller University, N.Y., N.Y.
‡‡‡Present address: Fermi National Accelerator Laboratory, Batavia, Illinois.
§§§Present address: Brookhaven National Laboratory, Upton, N.Y.

[1]M. L. Good and W. D. Walker, Phys. Rev. 120, 1857 (1960).
[2]J. W. Cooper *et al.*, Bull. Am. Phys. Soc. 22, 584 (1977).
[3]D. G. Fong *et al.*, Phys. Lett. 53B, 290 (1974).
[4]D. Fong *et al.*, Nuovo Cimento 34A, 659 (1976).
[5]D. Fong *et al.*, Nucl. Phys. B104, 32 (1976).
[6]D. Fong *et al.*, Nucl. Phys. B102, 386 (1976).
[7]T. B. Day, University of Maryland Report No. AEC-ORO-2504-100 Supplements, 1974 (unpublished).
[8]D. Brick *et al.*, Phys. Rev. D 18, 3099 (1978).
[9]J. Ballam *et al.*, Phys. Rev. D 4, 1946 (1971).
[10]The reaction $\pi^-p\to\pi^-\pi^-\pi^+p$ in the same data sample is discussed thoroughly in Ref. 4 and in A. E. Snyder, thesis, University of Illinois at Urbana-Champaign, 1975 (unpublished).
[11]D. Fong *et al.*, Phys. Lett. 60B, 124 (1975).
[12]R. Harris *et al.*, Phys. Lett. 59B, 187 (1975).